Gabrelian, Gabrelian; Ross, Glenn; Bespalova, Kristina; Paulasto-Kröckel, Mervi

Unlocking the Potential of Piezoelectric Films Grown on Vertical Surfaces for Inertial MEMS

Published in:
Materials Today Communications

DOI:
10.1016/j.mtcomm.2022.104522

Published: 01/12/2022

Document Version
Publisher's PDF, also known as Version of record

Please cite the original version:
Gabrelian, G., Ross, G., Bespalova, K., & Paulasto-Kröckel, M. (2022). Unlocking the Potential of Piezoelectric Films Grown on Vertical Surfaces for Inertial MEMS. *Materials Today Communications*, *33*, Article 104522. https://doi.org/10.1016/j.mtcomm.2022.104522

Materials Today Communications 33 (2022) 104522

Contents lists available at ScienceDirect

Materials Today Communications

journal homepage: www.elsevier.com/locate/mtcomm

Unlocking the potential of piezoelectric films grown on vertical surfaces for inertial MEMS

Artem Gabrelian [*,1], Glenn Ross, Kristina Bespalova, Mervi Paulasto-Kröckel

Department of Electrical Engineering and Automation, Aalto University, P.O. Box 13500, FIN-00076 Aalto, Finland

ARTICLE INFO

Keywords:
Mems
Gyroscope
Angular rate sensitivity
Finite element modeling
COMSOL
Aluminum nitride

ABSTRACT

Devices based on piezoelectric actuation are some of the most promising among the microelectromechanical systems (MEMS). Commonly, piezoelectric materials, such as aluminum nitride (AlN), are utilized to perform out-of-the-plane motion due to a clear and simple fabrication process. However, in-plane actuation is essential for inertial sensors, such as gyroscopes, where actuation and sensing directions are strongly perpendicular. Moreover, in-plane actuation and sensing can also find applications beyond inertial sensors. This paper presents the finite-element-modeling (FEM) of the MEMS gyroscope with the AlN thin films on vertical sidewalls that demonstrate in-plane actuation and unleash the full potential of piezoelectric AlN MEMS devices. Current work focuses on inertial sensing with the half-fork MEMS gyroscope's FEM simulation. This device has a significant advantage in scaling, while its output is in a competitive range among existing commercial angular rate sensors. The FEM simulations in COMSOL Multiphysics (COMSOL) allow to measure the angular rate sensitivity and perform further design optimization. Ultimately, this research shows the potential of the AlN sidewall structures in MEMS gyroscopes by optimizing the angular rate sensitivity in the range of [− 64.64] degrees per second (dps) with the peak value of 1 mV/dps.

1. Introduction

Emerging technology trends, such as the internet of things (IoT) or fifth-generation cellular network technology (5 G), have led to increased attention to MEMS sensors and actuators [1]. To meet the growing demand, existing MEMS devices should have improved characteristics, such as size, cost, reliability, and sensing output [2].

The actuation mechanism of the MEMS device could be generated by a wide variety of methods. Sensor's design includes thermal [3], electromagnetic [4], and electrostatic transduction [5]. Among these methods, piezoelectric actuation demonstrates significant advantages, mainly due to its high electromechanical coupling. This results in lower power consumption in piezoelectric devices, while electrostatically actuated sensors require an additional charge pump to increase their input voltage amplitude [6,7]. Currently, some of the most widespread piezoelectric materials in existing MEMS devices are aluminum nitride (AlN) and lead zirconate titanate (PZT). AlN is an environmentally friendly material with the availability to be compatible with the metal-oxide-semiconductor (CMOS) processes, which PZT does not have. These facts made AlN more promising in the design of vibration-based MEMS sensors.

Commonly, commercial inertial sensors are electrostatically actuated, while their sense output is measured by the capacitance change in sense direction [8]. However, recent studies show a significant range of published designs based on piezoelectric material properties. For instance, MEMS piezoelectric solid disk gyroscope was designed with an elliptic bulk acoustic wave mode [9]. Another piezo-based MEMS gyroscope utilizes a beam-based structure, where a piezoelectric layer is sandwiched between two electrodes [10].

Among AlN-based piezoelectric devices, the most common approach to utilize out-of-plane deflections by the sputtering deposition of AlN on a substrate. However, multi-axis sensors, such as gyroscopes, require perpendicular drive and sense directions, what creates a high demand for in-plane actuation. Moreover, enhanced in-plane actuation and sensing can also find their application beyond inertial sensors. Energy harvesters based on AlN could generate power by harvesting small magnitudes of energy from ambient vibrations. Implementation of the AlN sidewall structure will allow to generate voltage from in-plane

* Corresponding author.
E-mail address: artem.gabrelian@aalto.fi (A. Gabrelian).
[1] https://orcid.org/0000–0001-7742–4520

https://doi.org/10.1016/j.mtcomm.2022.104522
Received 13 July 2022; Received in revised form 30 August 2022; Accepted 19 September 2022
Available online 21 September 2022

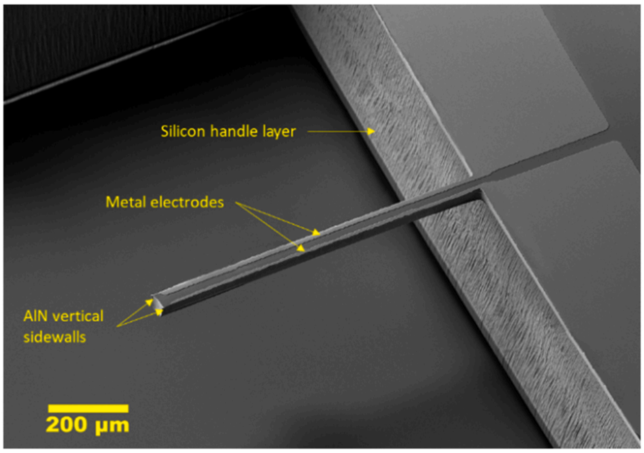

Fig. 1. Scanning Electron Microscopy (SEM) image of the released silicon cantilever with high-aspect-ratio AlN vertical sidewalls fabricated on SOI wafer with 50 μm device layer.

deflections and lead to the increased device's output. In addition, in-plane motion creates the opportunity to stack energy harvesters into a united array, which will multiply overall harvesting efficiency. At the same time, piezoelectric in-plane actuation could be attractive in high-quality switching of RF MEMS. The challenge with in-plane actuation and sensing is the deposition of the piezoelectric and electrode materials on the vertical sidewalls with high crystal quality. To overcome this, deposition has been achieved by metalorganic chemical vapor deposition (MOCVD) or atomic layer deposition (ALD) of the piezoelectric AlN and metal electrodes. [11,12]. Fig. 1 shows the SEM picture of the in-plane cantilever with the MOCVD deposited piezoelectric AlN sidewalls fabricated on a silicon-on-insulator (SOI) wafer. The main feature of this structure is the opportunity to utilize bimorph design by means of piezoelectric thin films on both sides of the cantilever. The voltage is applied over the AlN thin film sidewalls by contacts through the metal electrode's area for actuation. Following that, the proposed sidewall structure utilizes the increased area of metal electrodes, which even more improves the observable sensor's output.

In the current work, to fully understand the operating characteristics and the perspective of the MEMS design with vertical piezoelectric AlN thin-film structures, a comprehensive FEM study was undertaken. Multiphysics study allows the implementation of the properties of the anisotropic and piezoelectric materials and their coupling with the FEM software packages. To demonstrate the potential of the sidewall concept in an inertial sensing application, a COMSOL FEM simulation of the half-fork Coriolis vibrating gyroscope (CVG) with the piezoelectric AlN sidewall's structure was performed.

The proposed device's main characteristics, such as mechanical rate sensitivity and scaling, were calculated after simulations to estimate overall gyroscope performance. A significant amount of commercial and research-based MEMS gyroscopes allows for comparing the output of the modeled gyroscope presented in this work with the existing devices.

Geometry optimization was undertaken to investigate the potential performance of a sidewall-piezoelectric structure in MEMS. Multi-parameter characterization was performed in COMSOL to obtain the mechanical sensitivity for a range of the modified design options. Since the bimorph piezoelectric cantilever is the fundamental structure of the proposed MEMS gyroscope device, initial geometry parameters were assumed by considering fabricated samples of the released cantilever, shown in Fig. 1.

This paper's structure is presented as follows. Section 2 describes the operation principle of the half-tuning fork resonator. Section 3 includes the detailed FEM simulation with the modal analysis, Q-factor discussion, and sensitivity value calculation with the following geometry optimization. The paper is concluded in Section 4.

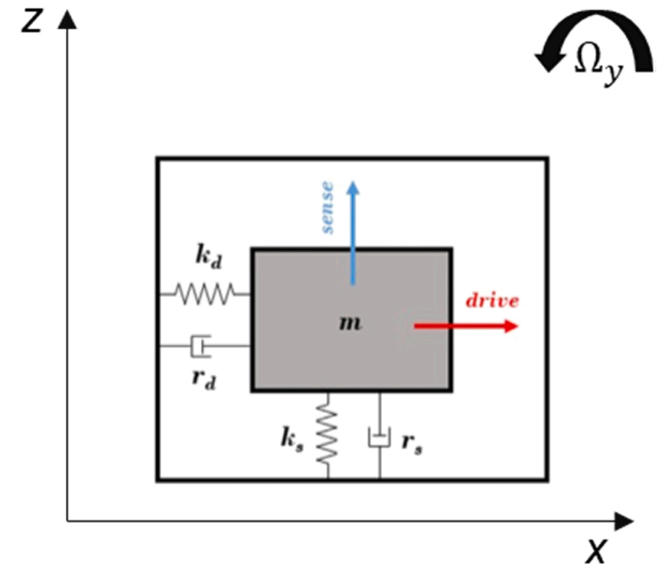

Fig. 2. Scheme of two spring-mass-damper systems of the MEMS vibratory gyroscope.

2. Methodology

MEMS vibrating gyroscope working principle is based on the Coriolis acceleration effect. When the movable proof mass is in resonance with the applied angular velocity, the Coriolis force generates the displacement in the direction perpendicular to the linear velocity [7].

A basic single-axis Coriolis vibrating gyroscope (CVG) could be described as a two-DOF resonator. It consists of two mass-spring-damper systems that are expressed by the equations of motion for both drive and sense axes:

$$m_d\ddot{x} + r_d\dot{x} + k_d x = F_d \sin(\omega t) \tag{1}$$

$$m_s\ddot{y} + r_s\dot{y} + k_s y = F_{cor} \tag{2}$$

where for drive direction: m_d is the mass, r_d – damping coefficient, k_d stiffness,and $F_d \sin(\omega t)$ is the applied force, while for sense: m_s, r_s, k_s, F_{cor} are the mass, damping coefficient, stiffness, and the Coriolis force applied in sense direction, respectively.

Coriolis force amplitude is expressed as follows:

$$F_{cor} = -2m(v_d \times \Omega_{ext}) \tag{3}$$

where m is the mass of the moving system, v_d – is the linear velocity and Ω_{ext} is the angular velocity. The lumped gyroscope system is illustrated in Fig. 2.

Components of motion from Eq. 1 and Eq. 2 could be contributed to the COMSOL FEA modeling as follows:

- m_d, m_s – the mass of the built geometry, material density
- r_d, r_s – presented in the model as a Rayleigh damping, values are based on Q-factor and resonant frequency (will be discussed in more detail in Section 3.3)
- k_d, k_s – stiffness for drive and sense modes corresponds to anisotropic properties of used materials (e,q, elastic, and compliance matrices) and physical constraints (fixed plane constraint)

The proposed design fully utilizes the piezo-cantilever structure, presented in Fig. 1. AlN vertical sidewalls are responsible for driving direction, causing in-plane motion of the cantilever. Piezoelectric thin films deform under applied external voltage, creating cantilever deflections with linear velocity in the drive direction. As shown in the lumped model in Fig. 2, sense direction is opposite to drive, and one can

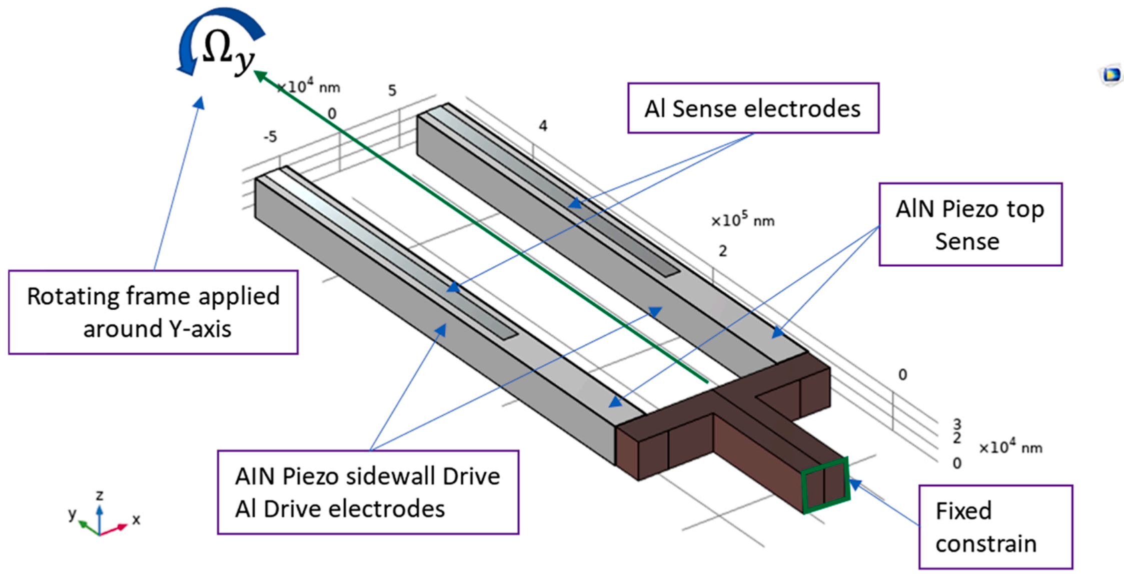

Fig. 3. The mechanical structure of the half-fork MEMS vibratory gyroscope.

achieve it by having out-of-the-plane motion on the same cantilever. Therefore, an angular velocity must be applied to observe deflections in the sense direction. Eventually, sense piezoelectric thin film located on the top of the cantilever transforms mechanical deformation caused by Coriolis force into the output voltage.

3. Results

3.1. FEA model configuration

Fig. 3 depicts a schematic view of the half-turning fork CVG based on manufactured AlN piezoelectric cantilevers shown in Fig. 1. The gyroscope of 160 μm in width and 420 μm in length with an overall thickness of 50 μm is made of 0.04 Ohm p-type silicon, which is also defined as a ground electrode. The mechanical structure of the resonator consists of two cantilevers connected between each other and with the deposited AlN layers. In addition, the following boundary conditions were applied to simulate the gyroscope rotation: a rotating frame around the Y-axis with a specified value of angular velocity *va* and a fixed constraint at the uniform end of the sensor's Z-X plane, as presented in Fig. 3.

To solve the FEA model that contains the anisotropic properties, it is required to determine the elastic constants. Experimentally obtained elastic-stiffness coefficients of the AlN wurtzite-type-structure are expressed with the following stiffness tensor [13]:

$$\begin{bmatrix} C_{11} & C_{12} & C_{13} & & & \\ C_{21} & C_{22} & C_{23} & & & \\ C_{31} & C_{32} & C_{33} & & & \\ & & & C_{44} & & \\ & & & & C_{44} & \\ & & & & & \frac{1}{2}(C_{11}-C_{12}) \end{bmatrix} = \begin{bmatrix} 410 & 149 & 99 & & & \\ 149 & 410 & 149 & & & \\ 99 & 149 & 389 & & & \\ & & & 125 & & \\ & & & & 125 & \\ & & & & & 130.5 \end{bmatrix} [GPa]$$

In addition, the corresponding stress-piezoelectric constant tensors were utilized to define modeled material as a piezoelectric [14].

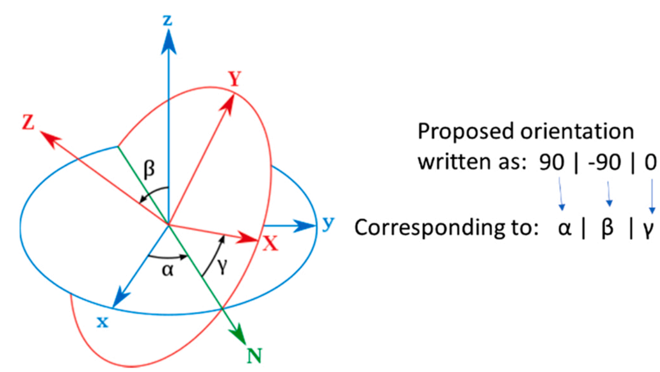

Fig. 4. Euler angles interpretation.

$$\begin{bmatrix} & & & & e_{24} & \\ & & & e_{24} & & \\ e_{31} & e_{31} & e_{33} & & & \end{bmatrix} = \begin{bmatrix} & & & & -0.48 & \\ & & & -0.48 & & \\ -0.58 & -0.58 & 1.55 & & & \end{bmatrix} \left[\frac{C}{m^2}\right]$$

In the proposed modeling, Al electrodes are located on each side of the cantilevers in order to simulate piezoelectric actuation. Two cantilevers oscillate in a counter-phase with the applied AC voltage on each drive electrode.

When the gyroscope oscillates at resonance along the X-axis, the rotating frame around Y-axis causes the displacement in the Z-axis direction from the Coriolis force. There are two Al electrodes on each cantilever to sense generated electrical signals from the deformed piezoelectric layer. Out-of-the-plane deflections have opposite directions. Thus, the difference in voltage between the two electrodes serves as an absolute sense output.

The proposed design separates drive and sense direction into X and Z axes, respectively. To obtain the correct behavior of the simulated model, two reference frames were created. Specimen frame (S_{xyz}) refers to the stationary coordinate system of the half-fork silicon base, while crystallographic (C_{abc}) frame shows the orientation of the AlN films. To observe separate drive and sense directions, drive crystallographic reference frames are rotated with respect to the specimen reference plane. The additional rotating systems were created to model the mentioned layers' orientation in COMSOL, while Euler angles configured axes switching. This model has 3 cases:

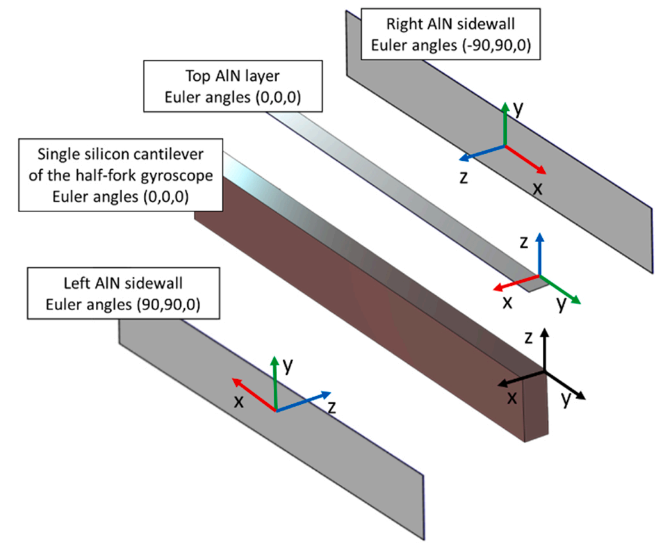

Fig. 5. Piezoelectric thin film orientation with the Euler angles usage in COMSOL.

- no rotation (sense AlN): $S_z||C_c$ (0,0,0)
- positive rotation (drive AlN): -$S_x||C_c$ (90,90,0)
- negative rotation (drive AlN): $S_x||C_c$ (−90,90,0)

Fig. 4 describes the used notation for setting up specified angles. In order to correct the sidewalls modeling, two rotating systems tilted to 90 degrees on β and 90 and $-$ 90 for α were created on the left and right sides, respectively. The overall breakdown of the piezoelectric layers' orientations is illustrated in Fig. 5.

Initial dimensions of the proposed design are shown in Fig. 6, while all geometry parameters are listed in Table 1.

3.2. Modal analysis

The eigenvalue solver from COMSOL Multiphysics uses the relation between complex eigenvalue and frequency to determine the mode shapes and value of natural resonant frequencies of the modeled gyroscope. The frequencies of interest are the drive mode (in-plane, X-axis) and the sense mode (out-of-the-plane, Z-axis). Resulted mode shapes of the half-tuning fork gyroscope's eigenfrequency simulation are presented in Fig. 7, and the resonant values are listed in Table 2.

The proposed design operates in a counter-phase to provide more accurate output with reduced quadrature error. Counter-phase mode was selected owing to its opportunity to efficiently utilize the differential output, which requires to have only two sense electrodes. In this case, the gyroscope's sensitivity constitutes the voltage difference between two cantilevers, because generated potentials have opposite signs.

Table 1
Nominal values of design parameters.

Parameter name	Value [μm]	Description
height	50	Height of the cantilever
width	20	Width of the cantilever
length	400	Length of the cantilever
AlN_thickness	0.300	Thickness of AlN
Al_thickness	0.3	Thickness of Al contacts
wf	35	Width of the fixed end
lf	100	Length between the fixed end and the fork base
lk	25	Length of the fork base
wk	160	Width of the fork base

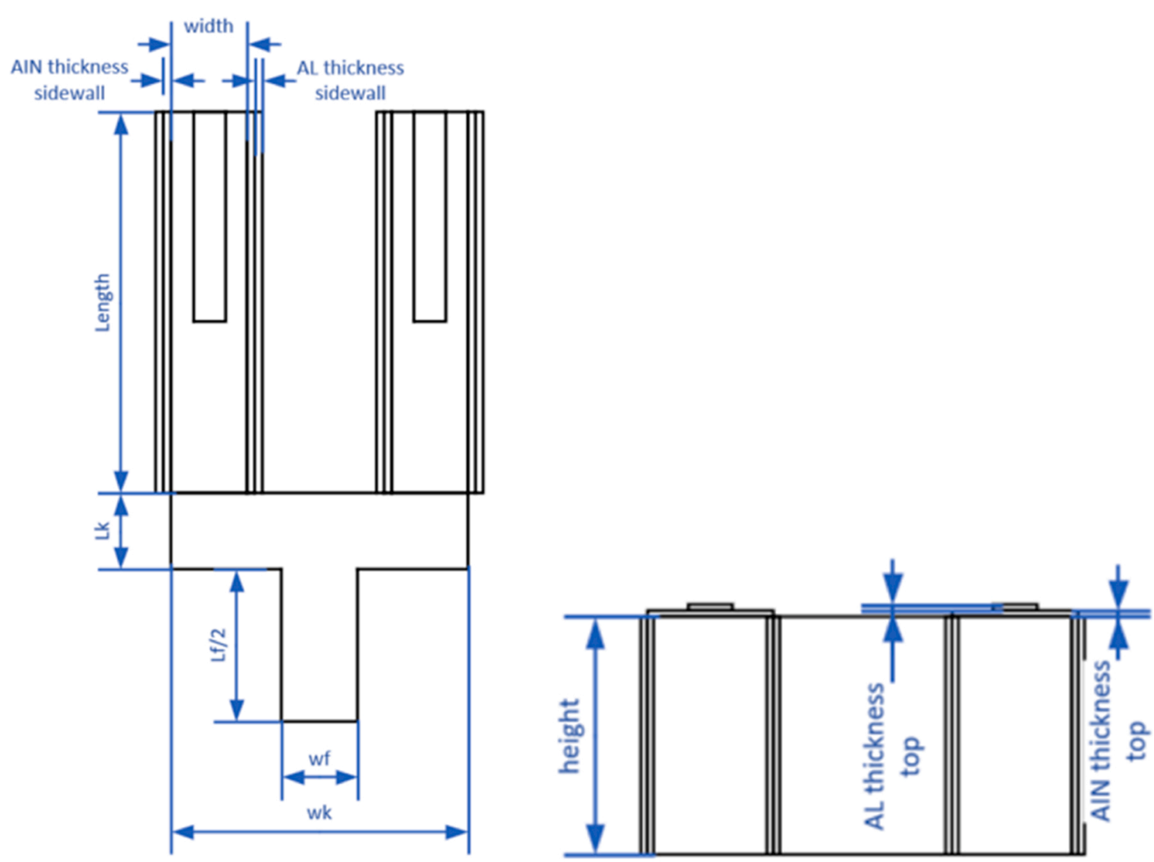

Fig. 6. 2-D view of the mechanical structure.

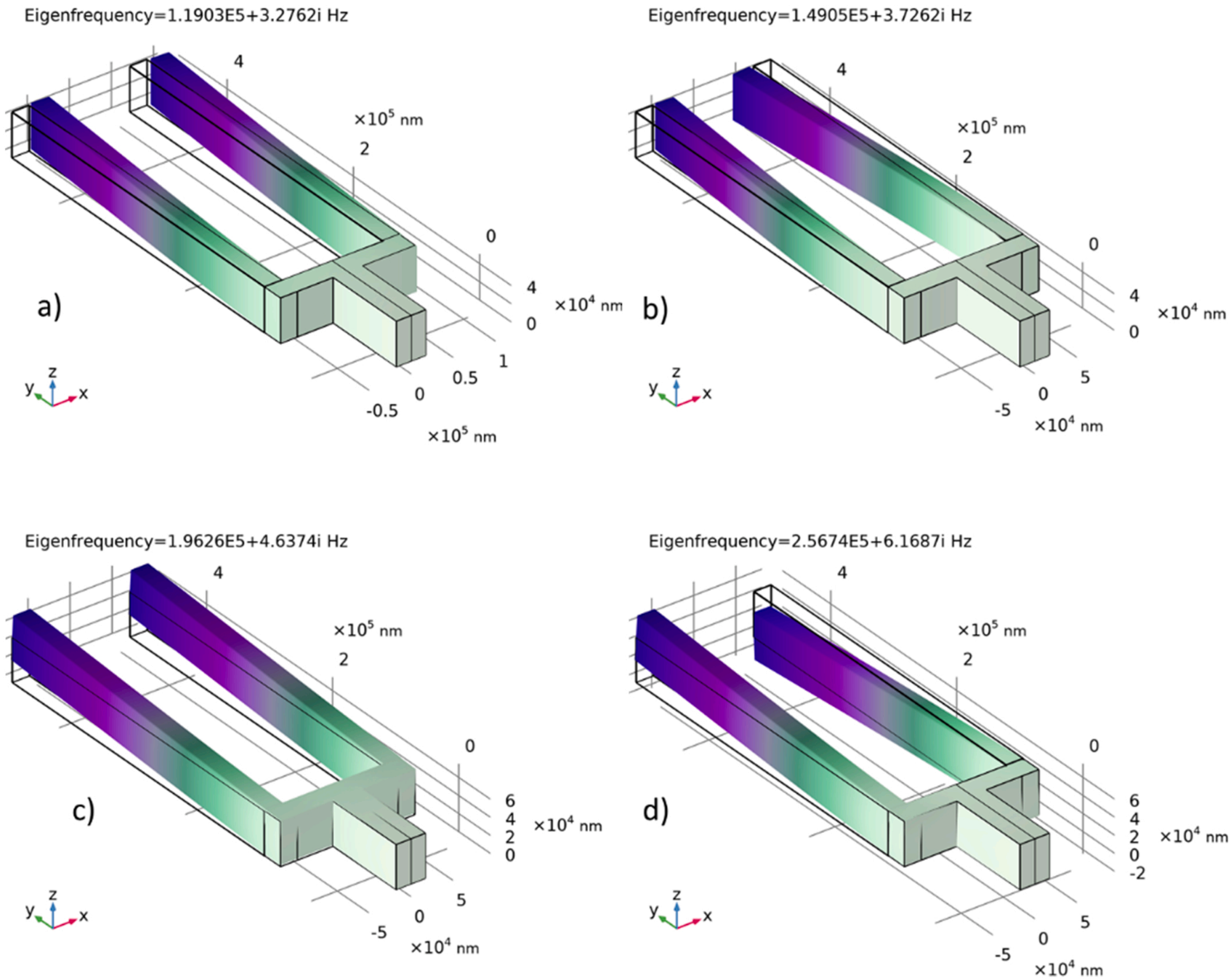

Fig. 7. Modal shapes of the half-tuning fork CVG. a) Drive in-phase mode. b) Drive counter-phase mode. c) Sense in-phase mode. d) Sense counter-phase mode.

Table 2
Resonant frequencies of the proposed design.

Modal Shape	Frequency [kHz]
Drive in-phase	119.03
Drive counter-phase	149.05
Sense counter-phase	196.26
Sense in-phase	256.74

While in in-phase mode sense voltage signs on each cantilever are equal, leading to the need for additional neutral electrodes and increased losses. Following that, the required operational frequencies are 149.05 kHz (Fig. 7b) and 256.74 kHz (Fig. 7d) for drive and sense modes, respectively.

3.3. Drive mode study

In this work, the drive mode of the proposed MEMS gyroscope is actuated by the converse piezoelectric effect. Both cantilevers of the resonator have AlN deposited thin film sidewalls with the Al electrodes on them. To increase drive displacement amplitude, AC voltage has a 180 phase difference on the sidewalls of the Al electrodes, while both cantilevers have mirrored orientation between each other to perform drive antiphase deflections. Fig. 8 shows the locations of the applied input voltage.

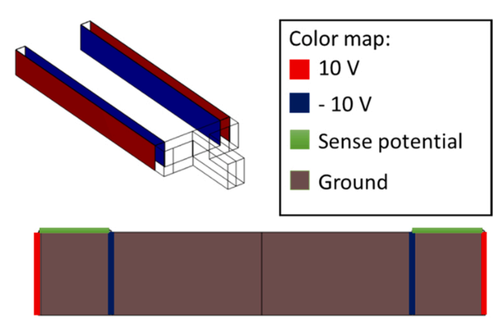

Fig. 8. Location of drive and sense Al electrodes. AC 10 V refers to drive electrodes, sense potential shows sense electrodes.

In practice, the drive input voltage amplitude is proportional to displacement amplitude. As a result, a higher source voltage results in a higher angular rate sensitivity. However, the maximum voltage amplitude is limited due to size and practical limitations. The majority of the commercial MEMS gyroscopes have input voltage amplitude between 10 and 30 V. Moreover, some devices contain charge pumps to increase the listed values [8,15]. The AC amplitude of 10 V was selected for the

Table 3
Drive mode parameters of resonance analysis.

Parameter Name	Value	Units	Description
va	64	deg/s	Angular velocity
beta	1.7797E-11	s	Rayleigh damping coef
alpha	31.217	Hz	Rayleigh damping coef
freq	149,050	Hz	Resonant frequency
Q	20,000	–	Quality factor
Voltage1	10	V	Drive voltage
Voltage2	-10	V	Drive voltage

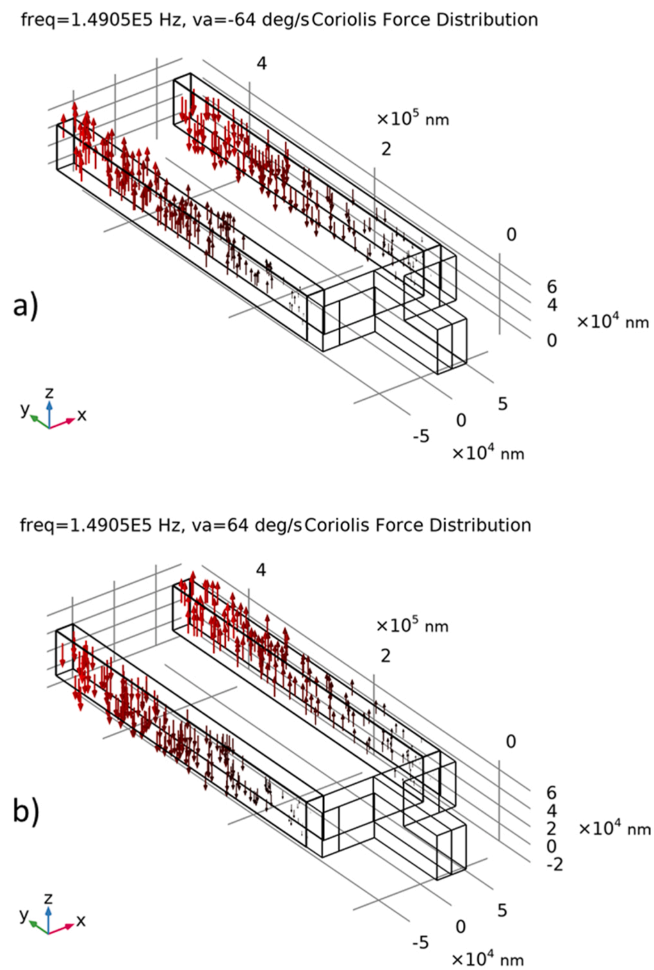

Fig. 9. Coriolis force distribution of the half-tuning fork gyroscope at a resonant frequency. a) Positive angular velocity applied. b) Negative angular velocity applied.

proposed CVG half-fork gyroscope to follow considered limitations.

Initially, the damping boundary condition is presented as a loss factor damping and could be set up as a single ratio. However, this option does not consider the difference in behavior between different resonant modes. Thus, Rayleigh damping was selected for further modeling to enhance the simulation results. It is expressed as a linear combination of the mass and stiffness matrices [16] and could be analytically calculated as follows:

$$C = \alpha_{dM} M + \beta_{dK} K \quad (4)$$

Parameter C in Eq. (4) is defined as a fraction of the mass and the stiffness using two parameters, α_{dM} and β_{dK}. The values of these constants can be derived from the values of drive frequency and quality factor Q_d [17].

MEMS gyroscopes require a high vacuum environment to improve their performance as with the other sensors such as accelerometers. These conditions are strongly interrelated with the resonator's structural behavior because the vacuum level affects the mechanical quality factor. The high-quality factor in the strongly encapsulated systems allows a more significant resonating displacement at lower input voltage [18,19]. Experimental measuring and testing for high-hermitized MEMS gyroscopes showed that their Q-factor value is in the range between 9840 and 34,000 [5,20]. In addition, in recent MEMS modeling works this parameter was assumed to be between 10,000 and 30,000 [21–23]. However, in analytical calculations for the high-quality sensors, Q-factor can even reach 50,000 [24]. Thus, the quality factor for the proposed simulation was estimated as 20,000, while the remaining parameters are presented in Table 3.

3.4. Angular rate sensitivity analysis

The mechanical or angular rate sensitivity was selected as an output value to estimate the potential of the simulated design. This parameter is presented in all devices with analog output and could be expressed as a relationship between output voltage (mV) and angular velocity (dps). One can determine sensitivity value by sweeping the range of angular velocities and calculating generated voltage by 1 dps velocity change.

To obtain a sensitivity value, COMSOL frequency-domain study was undertaken. With the fixed drive resonance frequency, the gyroscope was swept around different angular velocity values from − 64 dps to 64 dps with a step of 8 dps.

The simulated Coriolis force amplitude was analyzed for three different cases (positive, negative, and 0 rotating frames applied) to validate the correct behavior of the antiphase out-of-the-plane oscillations. Fig. 9 depicts the distribution of the Coriolis force component at a resonant frequency.

The correlation between the applied rotating frame and sense voltage was tested using FEM in COMSOL through the frequency-domain study. Fig. 10 provides the simulated dependence between the output voltage and angular velocity around Y-axis. Linear behavior of the received dependence allows evaluating mechanical rate sensitivity as a curve slope. Thus, the sensitivity value of the proposed gyroscope design constituted 0.013 mV/dps.

Overall, these results indicate that the achieved sensitivity value is already located in the lower border of the commercial range of MEMS gyroscopes. Moreover, the current design has a significant advantage in the case of geometrical scaling. The surface area parameter (multiplication of the device's length and width) was selected to obtain the quantitative scaling value. This characteristic contains not only crucial dimensions of the sensor but also can serve as a scaling parameter for the comparison of different MEMS devices. Fig. 11 shows an overview of the comparison between simulated gyroscope, existing commercial devices, and research prototypes in the case of angular rate sensitivity and scaling factor.

3.5. Geometry optimization

The optimization study aims to investigate the proposed gyroscope design with an AlN sidewall. Geometry optimization shows interrelated parameters and their contribution to the gyroscope's output. At the same time, improved sensitivity makes this design more competitive among existing gyroscopes with analog output. Fig. 11b illustrates the difference in scaling properties between the proposed and existing MEMS gyroscopes.

To study the possible improvements of the initial design, the model was parameterized. As mentioned before, gyroscope actuation is based on the piezoelectric effect, and AlN layers are concentrated on the gyroscope's cantilevers. Therefore, the following parameters for further optimization were selected: AlN thickness, height, and width of the cantilever. Table 4 depicts selected parameters and their sweeping range.

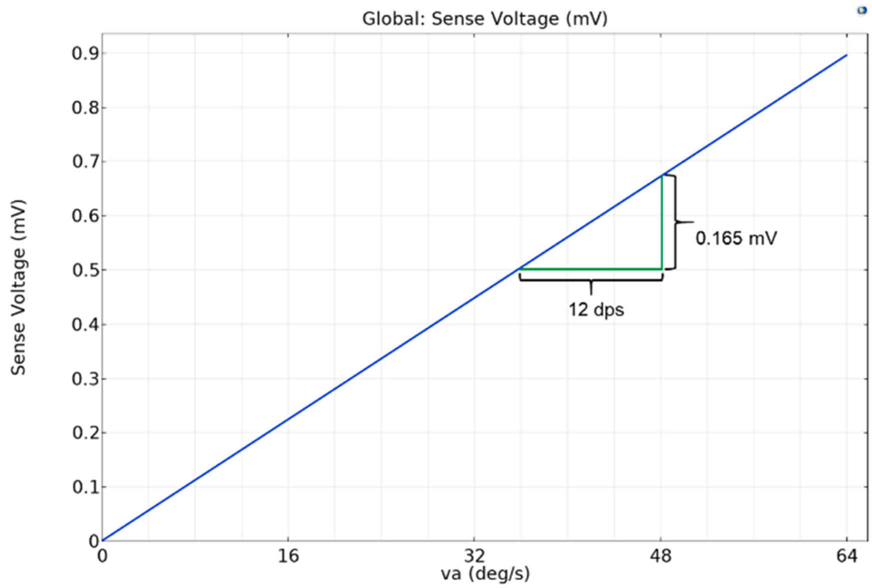

Fig. 10. Angular rate sensitivity output.

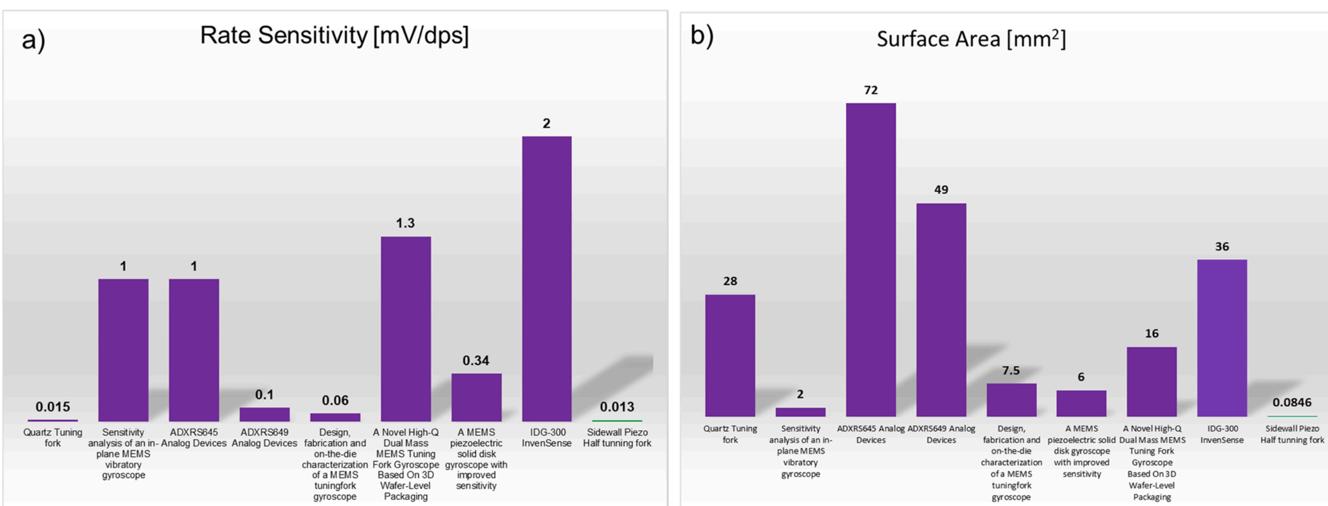

Fig. 11. Comparison of simulated half-fork MEMS gyroscope with the existing MEMS devices [8,9,15,21,24–27] a) Angular rate sensitivity. b) Scaling.

Table 4
Parameters selected for optimization and its sweeping range.

Parameter name	Value range [μm]	Description
height	28 30 42 54	Height of the cantilever
AlN_thickness	0.3 0.4 0.5 0.6	The thickness of the AlN top and sidewall layers
width	18 24 30 36	Width of the cantilever

3.6. *Resonance mode filtering*

At first, following the developed methodology, it is required to obtain the resonant frequencies for each gyroscope design. Thus, the COMSOL eigenfrequency study with the parameter sweep was performed to receive eigenmodes for all geometry combinations (Fig. 7). As discussed in Section 3.1, this model includes fixed plane boundary conditions, which will inevitably lead to the appearance of torsional and rotating eigenmodes. To exclude undesired modes and, at the same time to ensure that the required drive in-plane mode in antiphase (Fig. 7b) will appear after simulation, the desired number of eigenfrequencies in the COMSOL study properties was selected as 4.

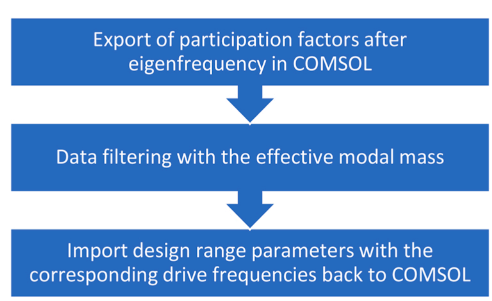

Fig. 12. Steps of eigenmodes filtering approach.

However, even a non-significant parameter range creates several modal frequencies (64 possible designs with 4 modes for each show 256 frequencies). In this case, manual selection of the desired mode behavior (Fig. 7) is not possible. The following filtering method, shown in Fig. 12,

Table 5
Parametric sweep samples in the frequency domain study in COMSOL (64 linear combinations total).

Parameter name	Values range sample	Parameter's units
height	54 28. 30 54	µm
AlN_thickness	500 400. 600 300	nm
width	30 30. 24 24	µm
freq	179,048.6039. 177,843.225	Hz

was developed to search the required mode efficiently.

Firstly, eigenfrequency study results and calculated participation factors were exported from COMSOL for further analysis. The desired drive modes have displacement in X-direction with the antiphase state of the cantilevers, while unwanted mode shapes contain twisting and rotation. Therefore, to exclude unnecessary mode shapes without manual sorting, built-in COMSOL participation factor and effective mass coefficients are used as filtering variables. Furthermore, we selected 64 frequencies from the initial dataset with the smallest effective modal mass in Z-direction and the highest participation factor in the X-direction for the angular rate sensitivity study. Then, the list of parameter ranges shown in Table 4 could be updated with the corresponding frequency value for each geometry design.

3.7. Scaling and sensitivity optimization

As shown in Section 3.5, to obtain angular rate sensitivity, it is required to plot a sense curve and calculate the gain in sense voltage per 1 dps change of angular velocity.

With the list of resonant frequencies obtained in the previous study, mechanical rate sensitivity can be calculated for each design option. Thus, the resonant frequency was added to the list of swept parameters, as shown in Table 5. All 64 geometry combinations were simulated at each own resonant frequency in this study.

The simulation showed that output results are susceptible to the cantilever geometry of the modeled gyroscope. The mechanical rate sensitivity varies between 0.0125 mV/dps to 1.21 mV/dps. Fig. 13 shows the sample of sensitivity curves based on the combination of frequency-domain study with applied rotating frame and parameter sweep for optimization.

Results of the performed simulation showed that the highest sensitivity values could be obtained at the lowest height and width but with the thickest AlN layer. Table 6 provides the simulation data of the 10 models with the highest sensitivity.

Further analysis was performed to validate the gyroscope's height impact on its sense output. It validated that some geometry parameters are more interrelated with the mechanical rate sensitivity than others. To observe how the values correlate with each other, the Pearson correlation coefficient (r-Pearson) was calculated. The Pearson correlation coefficient characterizes the existence of linear dependence between two values. Its value ranges from 1 to − 1, where 1 means a complete linear positive relationship, − 1 means a complete linear inverse

Table 6
Geometry parameters of the models with the highest sensitivity.

height [µm]	AlN_thickness [nm]	width [µm]	frequency [Hz]	Sensitivity [mV/dps]
28	600	24	165,375.26	1.214
28	500	24	164,562.58	0.750
28	400	24	163,620.26	0.510
28	300	24	162,525.95	0.335
30	600	30	178,258.07	0.238
30	600	24	165,663.58	0.228
30	500	30	177,718.27	0.227
30	400	30	177,321.17	0.210
30	500	24	164,765.41	0.190
30	300	30	176,803.56	0.186

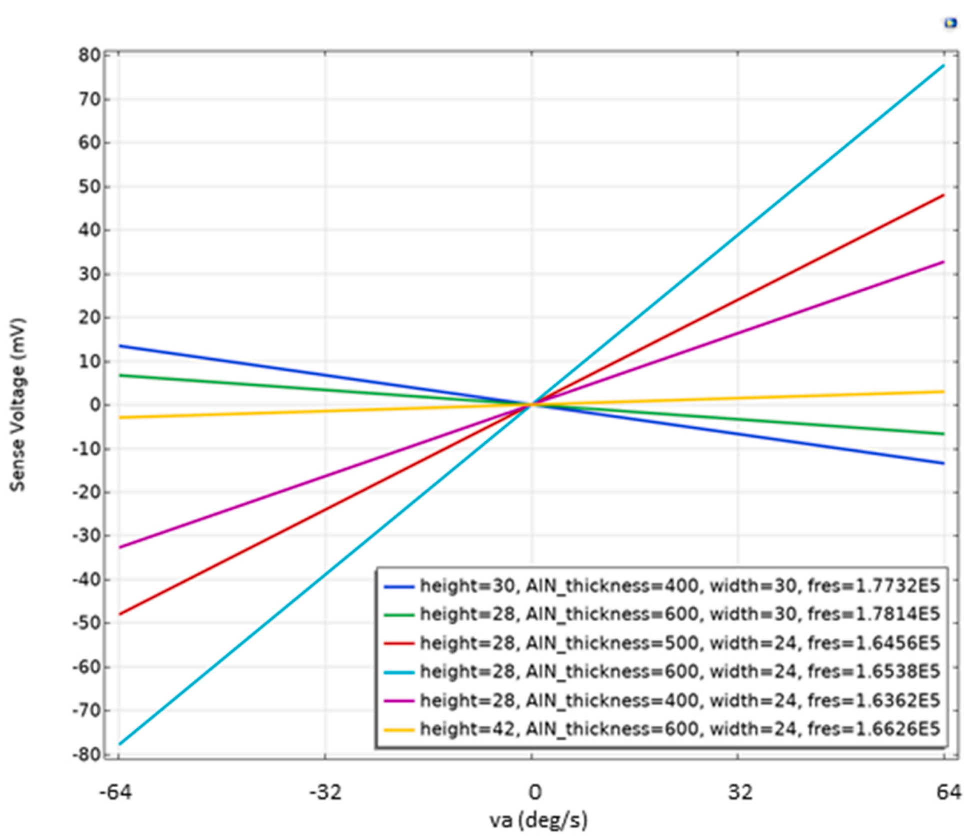

Fig. 13. Sample of the simulated sensitivity curves after optimization sweep.

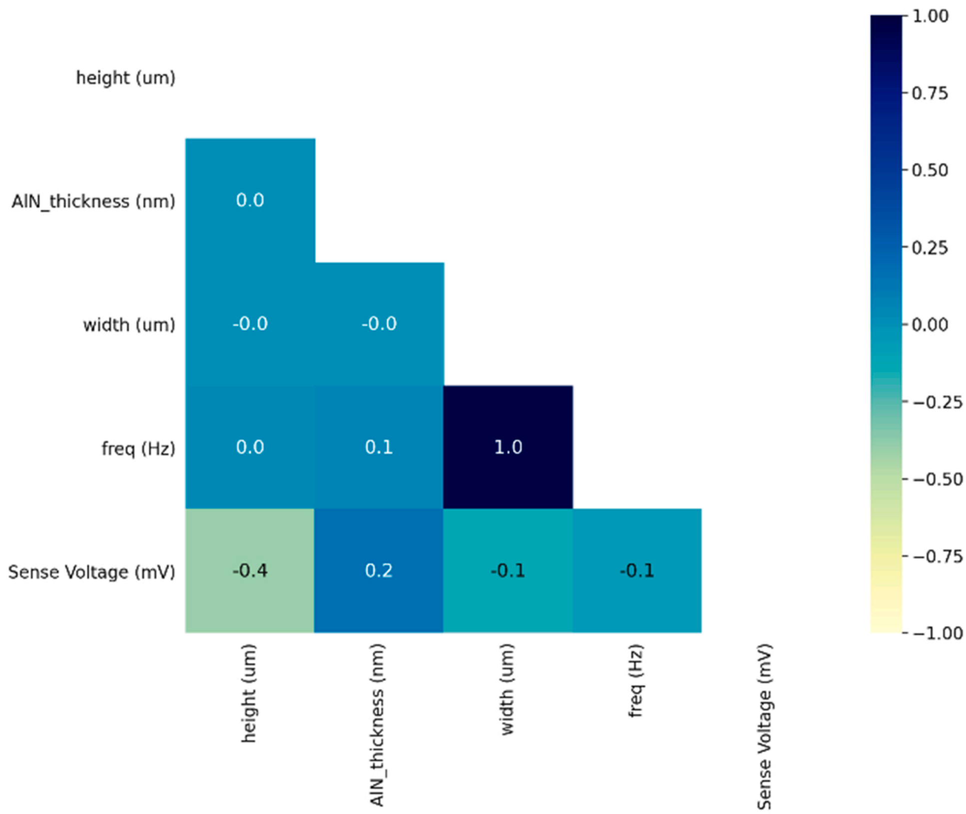

Fig. 14. Correlation matrix. Python with Pandas and Seaborn libraries.

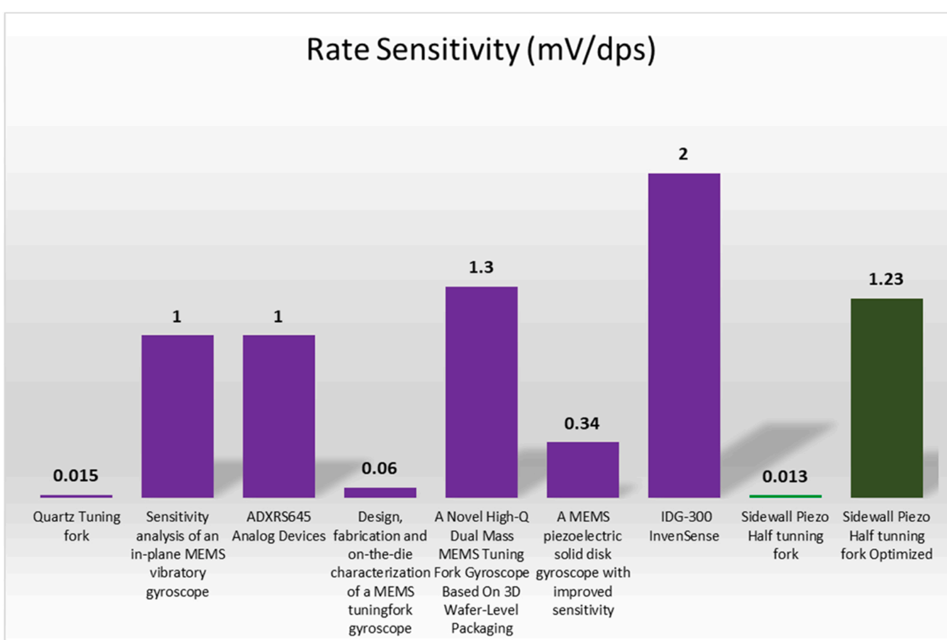

Fig. 15. Comparison of simulated half-fork MEMS gyroscope with the existing MEMS devices [8,9,15,21,24–27].

relationship, and 0 - no linear correlation. Fig. 14 shows the correlation matrix with the calculated Pearson correlation for each pair of parameters. Analysis revealed that the highest impact on the gyroscope's output has the cantilever's height (−0.4 Pearson's value), and AlN thickness has a smaller influence on sensitivity (0.2 Pearson's value), while the least parameters do not have any relevant correlation.

Obtained geometry dependences with the optimized simulations allow to analyze the potential improvements. Fig. 15 shows a comparison between the optimized gyroscope model and existing analog devices. Our model shows a significant increase in output sensitivity from an initial 0.013–1.23 mv/dps, what already in a comparable range with commercial devices.

4. Conclusion

The main goal of the current study was to investigate the potential of the AlN sidewall structure in the state-of-the-art MEMS design. A half-tuning fork gyroscope with the vertical AlN sidewalls was modeled to study how it couples with the inertial sensors. To analyze the proposed device's input, resonance, and output properties, FEM analysis was carried out by COMSOL Multiphysics, which includes eigenfrequency study, sensitivity analysis, and optimization.

In addition, the proposed FEM model provides a straightforward approach for comparison between the simulated gyroscope with the existing devices. Results showed that implementing the AlN sidewalls into the current piezoelectric-based MEMS design has a promising perspective. The initial model of the proposed MEMS gyroscope reached 0.013 mV/dps, which is within the lower limits of commercial devices. Despite the lower sensitivity values, the current design has a significant advantage in scaling factors. Square dimensions of the designed gyroscope are lower in several orders of magnitude compared to the existing research and commercial gyroscopes. The parameter characterization with the following optimization took place to make the proposed design more competitive in the case of angular rate sensitivity. FEM multi-parameter simulation showed that the design with a lower height and thicker AlN layer could reach the sensitivity value of more than 1.2 mV/dps.

Overall, this study contributes several ways to improve the understanding of AlN sidewall properties in the piezoelectric MEMS design. Achieved output values of the simulated gyroscope and its significant advantage in scalability provide a solid basis for the possible implementation of the piezoelectric sidewall structure beyond inertial sensor MEMS.

CRediT authorship contribution statement

Artem Gabrelian: Methodology, Investigation, Writing – original draft, Software. **Glenn Ross**: Conceptualization, Writing – review & editing, Supervision. **Kristina Bespalova**: Resources, Data curation. **Mervi PaulastoKröckel**: Supervision, Project administration, Writing – review & editing.

Declaration of Competing Interest

The authors declare that they have no known competing financial interests or personal relationships that could have appeared to influence the work reported in this paper.

Data availability

Data will be made available on request.

Acknowledgments

This work has been carried out as part of ECSEL18 Project NewControl, which receives funding within the Electronic Components and Systems For European Leadership Joint Undertaking (ESCEL JU) in collaboration with the European Union's Horizon2020 Framework Programme and National Authorities, under grant agreement N° 826653-2. The authors would like to acknowledge the Innovation Funding Agency Business Finland for their financial support. We acknowledge the provision of facilities and technical support of Aalto University at OtaNano Nanomicroscopy Center (Aalto-NMC).

Data availability

The data that support the findings of this study are available from the corresponding author upon reasonable request.

References

[1] J. Zhu, X. Liu, Q. Shi, T. He, Z. Sun, X. Guo, W. Liu, O. Sulaiman, B. Dong, C. Lee, Development trends and perspectives of future sensors and MEMS/NEMS, Micromachines 11 (7) (2020), https://doi.org/10.3390/mi11010007.
[2] N. Yazdi, F. Ayazi, K. Najafi, Micromachined inertial sensors, in: Proceedings of the IEEE, vol. 86, pp. 1640–1659, 1996. https://doi.org/10.1109/5.704269.
[3] M. Saqib, M. Mubasher Saleem, N. Mazhar, S. Awan, U. Shahbaz Khan, Design and analysis of a high-gain and robust multi-DOF electro-thermally actuated MEMS gyroscope, Micromachines 9 (577) (2018), https://doi.org/10.3390/mi9110577.
[4] I. Gebrel, L. Wang, S. Asokanthan, in Proceedings of the ASME 2018 International Design Engineering Technical Conferences and Computers and Information in Engineering Conference, vol. 8: 30th Conference on Mechanical Vibration and Noise, Quebec City, Quebec, Canada, August 2018.
[5] I. Faisal, D. Hussamud, L. Byeungleul, Single drive multi-axis gyroscope with high dynamic range, high linearity and wide bandwidth, Micromachines 10 (410) (2019), https://doi.org/10.3390/mi10060410.
[6] ADXRS642. Vibration Rejecting ±250°/s Yaw Rate Gyroscope. Data Sheet. ⟨https://www.analog.com/media/en/technical-documentation/data-sheets/ADXRS642.pdf⟩, Accessed March 2022.
[7] V. Kaajakari, Practical MEMS, Small Gear Publishing, Las Vegas, USA, 2009.
[8] ADXRS649. Fast Starting, ±20,000°/sec Vibration Rejecting Rate Gyroscope. Data Sheet. ⟨https://www.analog.com/media/en/technical-documentation/data-sheets/ADXRS649.pdf⟩, accessed: March 2022.
[9] C. Yuxiang, Z. Weiping, T. Jian, S. Dianjun, C. Wenyuan, A MEMS piezoelectric solid disk gyroscope with improved sensitivity, Microsyst. Technol. 21 (2015) 1371–1377, https://doi.org/10.1007/s00542-014-2344-z.
[10] K. Larkin, M. Ghommem, M. Serrano, A. Abdelkefi, A review on vibrating beam-based micro/nano-gyroscopes, Microsyst. Technol. 27 (2021) 4157–4181, https://doi.org/10.1007/s00542-020-05191-z.
[11] E. Österlund, S. Suihkonen, G. Ross, A. Torkkeli, H. Kuisma, M. Paulasto-Kröckel, Metalorganic chemical vapor deposition of aluminum nitride on vertical surfaces, J. Cryst. Growth 531 (125345) (2020), https://doi.org/10.1016/j.jcrysgro.2019.125345.
[12] E. Österlund, H. Seppänen, K. Bespalova, V. Miikkulainen, M. Paulasto-Kröckel, Atomic layer deposition of AlN using atomic layer annealing—towards high-quality AlN on vertical sidewalls, J. Vac. Sci. Technol. A 39 (032403) (2021), https://doi.org/10.1116/6.0000724.
[13] A. Wright, Elastic properties of zinc-blende and wurtzite AlN, GaN, and InN, J. Appl. Phys. 82 (1997) 2833–2839, https://doi.org/10.1063/1.366114.
[14] M. Levinshtein, S. Rumyantsev, M. Shur, Properties of Advanced Semiconductor Materials: GaN, AIN, InN, BN, SiC, SiGe, John Wiley & Sons, Hoboken, NJ, USA, 2001, pp. 31–47.
[15] ADXRS645 High Temperature, Vibration Rejecting ±2000°/sec Gyroscope. Data Sheet. ⟨https://www.analog.com/media/en/technical-documentation/data-sheets/ADXRS645.pdf⟩, Accessed: March 2022.
[16] S. Henrik, How to Model Different Types of Damping in COMSOL Multiphysics. ⟨https://www.comsol.com/blogs/how-to-model-different-types-of-damping-in-comsol-multiphysics⟩, Accessed: March 2022.
[17] COMSOL Multyphysics. MEMS Module. Application Library Manual. ⟨https://doc.comsol.com/5.3/doc/com.comsol.help.mems/MEMSApplicationLibraryManual.pdf⟩, Accessed: March 2022.
[18] C. Jeong, S. Seok, B. Lee, K. Hyeonched, C. Kukjin, A study on resonant frequency and Q factor tunings for MEMS vibratory gyroscopes, J. Micromech. Microeng. 14 (1530) (2004).
[19] B. Lee, S. Seok, K. Chun, A study on wafer level vacuum packaging for MEMS devices, J. Micromech. Microeng. 13 (663) (2003).
[20] A. Efimovskaya, Y. Yang, E. Ng, Y. Chen, I. Flader, T. Kenny, A. Shkel, in Proceedings of the 2017 IEEE International Symposium on Inertial Sensors and Systems (INERTIAL), Kauai, HI, USA, March 2017.
[21] K. Menon, J. Nayak, R. Pratap, Sensitivity analysis of an in-plane MEMS vibratory gyroscope, Micromachines 24 (2018) 2199–2213, https://doi.org/10.1007/s00542-017-3666-4.
[22] F. Lihui, Z. Ke, S. Yunan, C. Jianmin, C. Fang, Y. Aiying, A multi-fork Z-axis quartz micromachined gyroscope, Sensors 13 (2013) 12482–12496, https://doi.org/10.3390/s130912482.
[23] M. Rasekh, S. Khadem, Design and performance analysis of a nanogyroscope based on electrostatic actuation and capacitive sensing, J. Sound Vib. 332 (2013) 6155–6168, https://doi.org/10.1016/j.jsv.2013.06.024.
[24] P. Xu, C. Si, Y. He, Z. Wei, L. Jia, G. Han, J. Ning, F. Yang, A novel high-Q dual-mass MEMS tuning fork gyroscope based on 3D wafer-level packaging, Sensors 21 (6428) (2021), https://doi.org/10.3390/s21196428.
[25] Piezoelectric Rate Gyroscope. COMSOL 5.6, ⟨https://www.comsol.fi/model/download/775201/models.mems.piezoelectric_rate_gyroscope.pdf⟩, accessed: March 2022.
[26] J. Reddy, R. Pratap, Design, fabrication and on-the-die characterization of a MEMS tuning-fork gyroscope, ISSS J. Micro Smart Syst. 7 (2018) 87–96, https://doi.org/10.1007/s41683-018-0030-6.
[27] IDG-300. Integrated Dual-Axis Gyroscope. Data sheet. ⟨https://www.sparkfun.com/datasheets/Components/IDG-300_Datasheet.pdf⟩, Accessed: March 2022.